Department of Physics and Astronomy
University of Heidelberg

Bachelor Thesis in Physics
submitted by

Philipp Schultzen

born in Lübeck (Germany)

2018

Observation of $\Lambda_b^0 \to J/\Psi\Lambda^0\Phi$ at LHCb using 13 TeV Run 2 data and an evaluation of datataking methods with a view to Run 3

This Bachelor Thesis has been carried out by Philipp Schultzen at the

Physikalisches Institut in Heidelberg

under the supervision of

Dr. Sebastian Neubert

ABSTRACT

In this analysis the two data-taking methods Full stream and Turbo stream are compared for the decays $\Lambda_b^0 \to J/\Psi\Lambda^0\Phi$ (sig) and $\Lambda_b^0 \to J/\Psi\Lambda^0$ (ref) in 2016 data. This is the first observation of these decay channels in Run II data. The yield ratios $\frac{N_{sig}}{N_{ref}}$ are measured as 0.0025 ± 0.0005 and 0.0026 ± 0.0005 for Full Stream and Turbo Stream respectively, which validates the use of the Turbo stream on a complex decay topology, containing long living hyperons. Additionally the branching fraction of $\Lambda_b^0 \to J/\Psi\Lambda^0\Phi$ was measured relative to $\Lambda_b^0 \to J/\Psi\Lambda^0$ as $(5.9 \pm 1.1)\%$.

Finally upgrade MC is used to implement TurboSP lines for $\Lambda_b^0 \to J/\Psi\Lambda^0\Phi$, $\Lambda_b^0 \to J/\Psi\Lambda^0$ and $\Xi_b^- \to J/\Psi\Lambda^0 K^-$. The efficiency for the HLT2 emulation and subsequent reconstruction is 9.4 %, 17.5 % and 17.8 % respectively. The signal rate is estimated for $\Lambda_b^0 \to J/\Psi\Lambda^0$ as 0.3 Hz, while the background rate is 344 Hz. Using exclusive lines results in a reduction of the background rate to 47 Hz, 94 Hz and 109 Hz respectively.

ZUSAMMENFASSUNG

In dieser Analyse werden die zwei Methoden Full stream und Turbo stream anhand von 2016 Daten der Zerfälle $\Lambda_b^0 \to J/\Psi\Lambda^0\Phi$ (sig) und $\Lambda_b^0 \to J/\Psi\Lambda^0$ (ref) verglichen. Das ist die erste Untersuchung der Daten von Run II für diese Zerfälle. Das Verhältnis der Fitresultate $\frac{N_{sig}}{N_{ref}}$ ergibt 0.0025 ± 0.0005 und 0.0026 ± 0.0005 für Turbo stream und Full stream, was die Benutzung des Turbo streams an einem Zerfall mit komplexer Topologie validiert, welcher Hyperonen enthält. Zusätzlich wurde das Verzweigungsverhältnis von $\Lambda_b^0 \to J/\Psi\Lambda^0\Phi$ relativ zu dem von $\Lambda_b^0 \to J/\Psi\Lambda^0$ gemessen. Das relative Verzweigungsverhältnis wurde gefunden als $(5.9 \pm 1.1)\%$.

Zuletzt wurde Upgrade MC genutzt um die TurboSP Trigger Selektion für $\Lambda_b^0 \to J/\Psi\Lambda^0\Phi$, $\Lambda_b^0 \to J/\Psi\Lambda^0$ und $\Xi_b^- \to J/\Psi\Lambda^0 K^-$ zu implementieren. Die Effizienzen der Trigger Emulation und offline Rekonstruktion sind jeweils 9.4 %,17.5 % und 17.8 %. Die Signal Rate für $\Lambda_b^0 \to J/\Psi\Lambda^0$ wird geschätzt als 0.3 Hz, während die Hintergrundrate 344 Hz beträgt. Mit der Benutzung von exklusiven Trigger Selektionen kann die Rate auf jeweils 47 Hz, 94 Hz und 109 Hz gesenkt werden.

Contents

1 Introduction

The most successful model describing fundamental particles and their interactions is the standard model, which describes the fundamental interaction of the electromagnetical, weak and strong force between quarks and leptons by gauge bosons. The last missing fundamental particle, the Higgs boson was discovered in 2012 by ATLAS and CMS [1] [2]. In chapter 2 a short description of the standard model is given, introducing the fundamental forces and particles.

According to the standard model, as well as known states like mesons and baryons, pentaquarks could exist. Pentaquarks were already predicted by Murray Gell-Mann in 1964 [3]. The search for pentaquarks experienced a huge uprise by the discovery of two possible pentaquark candidates in the $J/\Psi p$ subsystem of the decay channel $\Lambda_b^0 \to J/\Psi p K^-$ by the LHCb Collaboration [4] in 2015. The two resonances $P_c^+(4380)$ and $P_c^+(4450)$ were found by an amplitude analysis with a significance of more than nine σ. An overview over pentaquark searches is given in chapter 3.

If these resonances containing a minimum quark content of $c\bar{c}uud$ really are pentaquarks, it is also expected to find candidates with a slightly different quark content such as $c\bar{c}uds$. One possible decay where this resonance could be observed is $\Lambda_b^0 \to J/\Psi\Lambda^0\Phi$, which motivates the observation of this channel. The feynman diagram can be seen next to the one of the first observed pentaquark in Figure 1.1.

Since a lot of events are detected at LHCb, the trigger has to filter and process a huge amount of data. To face the problem of limited bandwidth and higher multiplicities for Run II the data-taking method Turbo stream was implemented, which should replace the established Full stream method used for Run I. Main novelties of the Turbo stream are the use of the online reconstruction and a selective storage of data, which should further reduce the resulting bandwidth. More informations about the LHCb detector and trigger are shown in chapter 4. Since the channel $\Lambda_b^0 \to J/\Psi\Lambda^0\Phi$ is of interest for pentaquark searches , it needs to be established, before an amplitude analysis can be done. An important step to establish this channel is the measurement of the branching fraction relative to a reference channel. Therefore the reference channel $\Lambda_b^0 \to J/\Psi\Lambda^0$ is
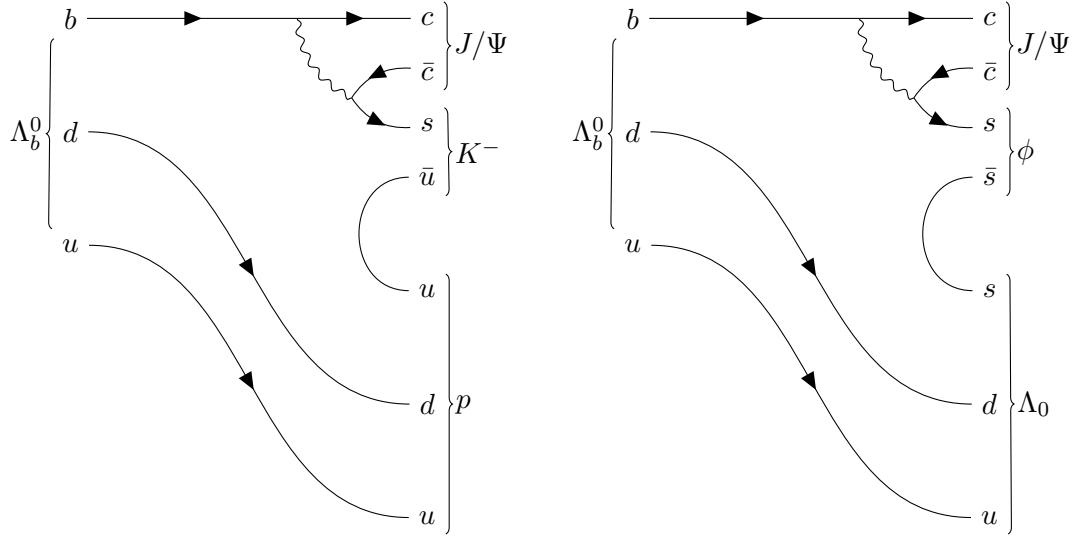
Figure 1.1: The feynman diagrams for $\Lambda_b^0 \to J/\Psi p K^-$ (left) and $\Lambda_b^0 \to J/\Psi \Lambda^0 \Phi$ (right).

chosen.

In this analysis the yields of 2016 data for both data taking methods Full stream and Turbo stream are measured and compared for the decay channels $\Lambda_b^0 \to J/\Psi \Lambda^0 \Phi$ and $\Lambda_b^0 \to J/\Psi \Lambda^0$ with the goal to verify the use of the Turbo stream and its online reconstruction. This is a first observation of Run II data within these channels.

In a next step simulated data of 2015 is used for an efficiency correction of the yield ratio of the Full stream, which results in a first branching fraction ratio measurement for this channel including Run II data. The ratio is then compared to the measured branching fraction ratio using Run I data [5].

Finally simulated data for the upgrade is used to develop a selection for the channels $\Lambda_b^0 \to J/\Psi \Lambda^0 \Phi$, $\Lambda_b^0 \to J/\Psi \Lambda^0$ and $\Xi_b^- \to J/\Psi \Lambda^0 K^-$ for the Turbo stream and the resulting efficiencies and used bandwidth are calculated.

2 Standard model

The standard model is a quantum field theory which connects elementary particles and three of the four fundamental forces (weak, strong and electromagnetic forces, gravitation is not included)[6]. It was developed in the second half of the twentieth century and was capable of not only describing all known elementary particles, but also of predicting phenomena and particles precisely. The top quark for example was predicted in 1973 [7] and confirmed in 1995 [8], the Higgs boson is another example. Experimental verification of those predictions led the standard model to become the established model of particle physics.
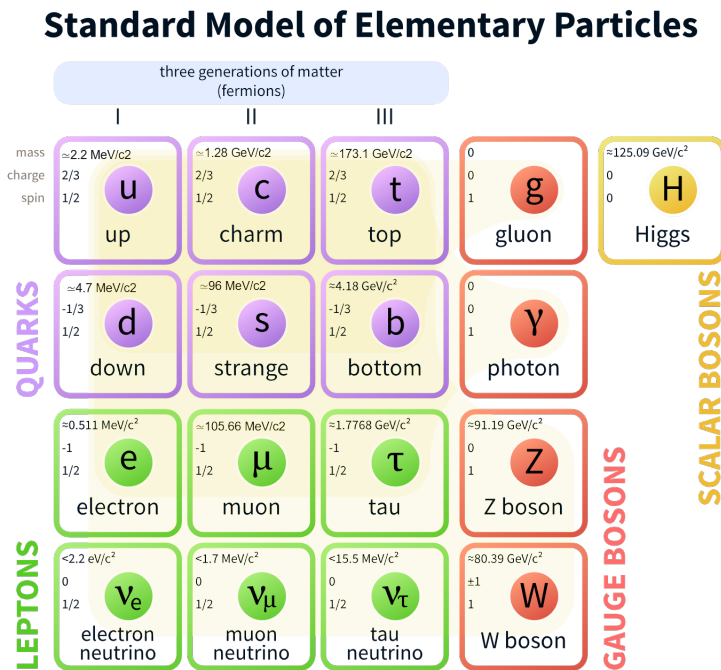
Figure 2.1: The fundamental particles of the standard model [9]

2.1 Fundamental particles and forces

In Figure 2.1 the fundamental particles of the standard model are shown. All matter is made of those particles. For every particle also an anti-particle exists with same mass and opposite flavors.

Particles can be divided in two groups, fermions and bosons.

Fermions have a half-integer spin and follow the fermi-dirac statistic. According to the Pauli exclusion principle, every microscopic state can only be occupied by a maximum of one fermion. The total wavefunction for fermions is antisymmetric.

Bosons have an integer spin, a symmetric wavefunction and their distribution in phase space is described by the bose-einstein statistic.

The two main groups of fermions, quarks and leptons, consist each of 6 different particles which are divided in 3 generations. They all have a spin of $\frac{1}{2}$. Only the first generation with the lightest masses and long lifetimes is stable. In contrast to leptons, quarks have color charge and thus can interact by the strong force. The four gauge bosons have a spin of 1 and are the force carriers, which mediate the respective forces.

The electromagnetic force

The electromagnetic force couples on the particle's charge. Its range is infinite but the force decreases by distance r with $\frac{1}{r}$. The interaction is mediated by photons. For detectors like LHCb the electromagnetic force is very important, because it is the only means to detect charged particles by interactions with detector material.

The weak force

The weak force is several magnitudes smaller than the electromagnetic force and the strong force. It is mediated by W and Z bosons and the only fundamental force capable of changing the flavor of quarks. This property makes the weak force very special and essential for many phenomena. The decay observed in this analysis is also only possible due to flavorchange (The Feynman-diagram is shown in Figure 1.1).

The strong force

The quantum field theory describing strong interaction is called *Quantum Chromodynamics* (QCD). The strong force is mediated by gluons. It is the strongest force and responsible for the binding of protons or neutrons. It acts on color charge, which is a quark property, thus only quarks or particles containing quarks interact strongly. Pos-

sible colors are red, green and blue for quarks and anti-red anti-green and anti-blue for antiquarks. The color is important due to a phenomenon called color confinement.

Color confinement or simply confinement describes the appearance of color carrying particles only in color-neutral states, so-called *hadrons*. This makes the strong force very special, because its fundamental particles, the quarks and gluons, do not occur isolated. This results in difficulties in measurements and theoretical predictions, e.g. the masses of exited states are not yet fully understood.
The hadrons which mostly occur are baryons and mesons. Baryons contain three quarks with different colors. The proton for example is a stable baryon containing two up- and one downquark. Mesons consist of a quark antiquark pair of matching color and anti-color.
Also compatible with the confinement are states with more quarks such as pentaquarks consisting of four quarks and one antiquark.

Taking spin and quark content into account, particles are grouped into multiplets. The $S = \frac{1}{2}$ baryon octet for baryons containing a combination of up, down and strange quarks is shown in Figure 2.2.
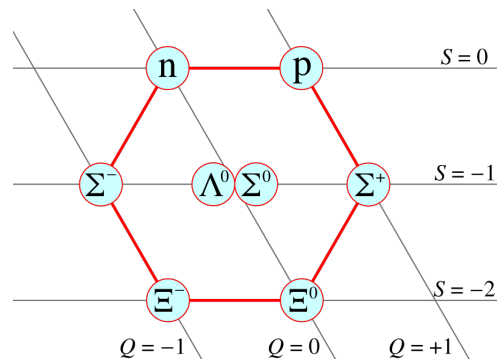
Figure 2.2: The $S = \frac{1}{2}$ baryon octet [10].

Since the first pentaquark with a minimal quark content of *c̄cuud* was found at LHCb [4], the fact, that particles occur in multiplets, motivates the search for a pentaquark including a strange quark.

The higgs field

The last missing particle, the Higgs boson, was found in 2012 at CERN [1] [2]. In the standard model, the Higgs boson and the higgs field explain the masses of the gauge

bosons and fermions.

3 Pentaquark searches

According to the standard model a state of four quarks and one anti-quark is capable of hadronization. The first prediction was by Murray Gell-Mann in 1964 [3]. He described the known mesons (q$\bar{q}$) and baryons (qqq) as only the lowest possible configurations and introduces possible baryon and meson states with a configuration of qqqq$\bar{q}$ and qq$\bar{q}\bar{q}$ respectively. The name *pentaquark* was introduced in 1987 by Harry J. Lipkin [11]. Searches for pentaquark states increased by the time due to continuous improvement in accelerator technology and center of mass energies. The Θ^+ pentaquark, which would consists of uudd$\bar{s}$, was the first pentaquark which was claimed to be observed. It was found by Takashi Nakano in 2003 [12] followed by other groups confirming its existence. In 2005 the Nature journal published an analysis with far more statistics of the Thomas Jefferson National Accelerator Facility, which could not observe this state [13].
In 2015 the LHCb Collaboration published an observation of two pentaquark candidates $P_c^+(4380)$ and $P_c^+(4450)$ [4]. These resonances were found by an amplitude analysis in the J/Ψp subsystem of the decay $\Lambda_b^0 \rightarrow J/\Psi p K^-$ thus containing a minimal quark content of $c\bar{c}uud$. With a significance of more than nine sigma, this observation is known as the first observation of a pentaquark.

The pentaquark of interest in this analysis has a minimal quark content of $c\bar{c}uds$, thus differs from the one above by a strange quark instead of an up quark. A. Feijoo et al. investigated the decay $\Lambda_b^0 \rightarrow J/\Psi\Lambda^0\eta$ and argued that this pentaquark could leave a signature in the invariant mass spectrum of the J/$\Psi\Lambda^0$ subsystem [14]. Lu et al. predicted a stable peak in the J/$\Psi\Lambda^0$ system in the decay $\Lambda_b^0 \rightarrow J/\Psi\Lambda^0 K^0$ [15].
The observed decay in this analysis is $\Lambda_b^0 \rightarrow J/\Psi\Lambda^0\Phi$. The prior observations in the J/$\Psi\Lambda^0$ subsystems of similar decays motivate the search for a pentaquark with a minimal quark content of $c\bar{c}uds$ within this channel. Furthermore, structures in the subsystems $\Lambda\Phi$ and $J/\Psi\Phi$ can occur. Since LHCb found exotic mesons in the $J/\Psi\Phi$ subsystem of the decay $B^+ \rightarrow J/\Psi\Phi K^+$ [16], these subsystems might also be of interest. The challenge in comparison to the already discovered pentaquark is the complexity of the decay. With the J/Ψ triggered by a $\mu^+\mu^-$ pair the resonances $P_c^+(4380)$ and $P_c^+(4450)$

were found in a decay constructed out of four final particles. In the decay observed in this analysis the Λ^0 is reconstructed by the most common decay into $p\pi^-$ (According to the Particle Data Group (PDG) the decay fraction for $p\pi^-$ is $(63.9 \pm 0.5)\%$ [17]). With Φ decaying mostly into K^+K^- $((48.9\pm0.5)\ \%)$ six final states occur in this channel.

4 The LHCb experiment

4.1 Detector

LHCb is one of the four big experiments at the Large Hadron Collider (LHC) in Geneva. It is designed for high precision measurements of CP violations in B decays. The high momentum and position resolution combined with an excellent particle identification system results in an unprecedented detection of B-baryons, which is why LHCb is the right place for exotic spectroscopy like the search for pentaquarks. It was running from 2010 to 2012 (Run I) and will run from 2015 to the end of 2018 (Run II). In 2021 Run III will start. In Figure 4.1 the LHCb detector for Run II is shown. Since beauty quarks enclose only a small polar angle with the beam, the LHCb detector is built as a single arm forward spectrometer. Its construction can be grouped into five main parts.

Tracking The Vertex Locator (VELO) measures the coordiantes of the primary vertex, where the p-p collision takes part, and further displaced vertices of subsequent decays. The tracking detectors TT behind the VELO and the detectors T1, T2 and T3 do a high precision measurement of hits for charged particles [18]. In the reconstruction this is later combined with the information about the vertices to form tracks.

Magnet An enourmous magnet consisting of two 27 tonnes heavy coils creates an integrated magnetic field of 4 Tm to measure momenta up to 200 GeV/c. In the magnetic field positive and negative charges move in opposite direction, so additional to the momenta also the charge sign can be measured [19]. The force F, that acts on particles with the charge q and velocity $\vec{v}$ in a magnetic field $\vec{B}$, is the Lorentz force.

$$F = q \cdot \vec{v} \times \vec{B} \tag{4.1}$$

Cherenkov Detectors The Ring-Imaging Cherenkov systems RICH1 and RICH2 are used for particle identifications. Their functionality is based on the phenomenon of cherenkov radiation, which occurs, when the particle's speed v is higher than the speed of light in the medium. Similar to the mach cone appearing by velocities higher than

the speed of sound, light is emitted under a certain angle Θ_c.

$$\cos(\Theta_c) = \frac{1}{n\beta} \tag{4.2}$$

Here β is defined as $\beta = \frac{v}{c_0}$ with the speed of light in vacuum c_0 and n the refractive index .

Regarding the cherenkov radiation, the RICH systems give a likelihood for the most common particles, e.g. K, p and π, comparing the radiation to the theoretical radiation with the particle masses.[20]

Calorimeters The most important calorimeters in the detector are the ECAL and HCAL. They are built of alternating metal and plastic layers. The Eletromagnetic Calorimeter (ECAL) measures the energy of light particles like photons or electrons. When these particles hit the ECAL they produce an electromagnetic shower due to pair production and bremsstrahlung. The secondary particles created in the shower now excite molecules in the plastic plate, which emit UV light. The amount of emitted radiation is proportional to the incoming particle energy, thus we can measure it by measuring the UV light emitted by the ECAL.

The Hadronic Calorimeter (HCAL) works like the ECAL but is optimized for hadrons like protons and neutrons. [21]

Muon system Many beauty decays present muons in the final states. Therefore a precise detection of muons is necessary. The Muon system consists of five rectangular stations, which are divided in small gas filled chambers. The reaction of the muons with the gas results in a decision for every chamber, whether a muon passed or not. Hence every station gives spatial coordinates of the muons, which can be combined to muon tracks. [22] [23]

4.2 The LHCb trigger and offline processing

Since there is a lot of data ($\sim$ 1 TB/s) coming from the LHCb detector and about 40 million collisions occur every second, it is very difficult to filter and process the huge amount of data in the corresponding time. Not only the fast processing time but even more important the bandwidth are the main bottlenecks, the LHCb trigger has to face. To maximize the data taking efficiency this task is solved by a data flow using many different steps before the data is ready for an analysis.
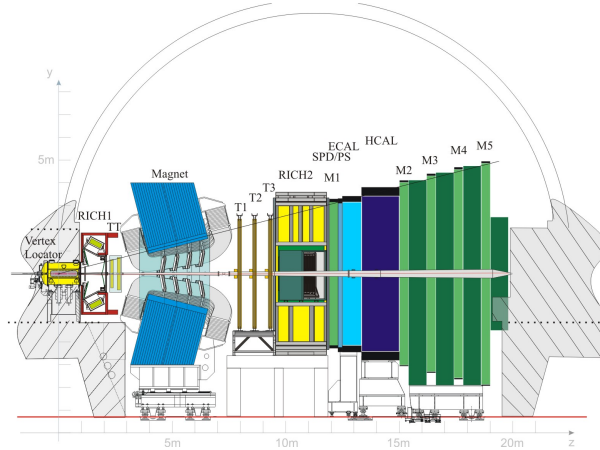
Figure 4.1: The LHCb detector for Run II [24].

Data coming from the proton proton collision has to pass the hardware trigger L0 (Level zero trigger) and then the High Level Triggers HLT1 and HLT2.

The decision, if an event is accepted and passed to the next trigger, is made by so called trigger lines (L0, HLT1 and HLT2 lines). An event is stored, if it passes the selection of at least one HLT2 line.

L0 is running synchronously to the 40 MHz bunch crossing signal of the LHC. It is subdivided into three components: The pile-up system, the muon trigger and the calorimeter trigger. In this analysis the decays are triggered by J/Ψ, which decays into two muons, thus the muon trigger is of interest. Among others, it measures the transverse momentum P_T and the total momentum P of all muons passing through the detector. Most L0 lines let the event pass, if the maximal measured P and P_T are above a certain threshold. The data flow rate is reduced to 870 kHz.

The HLT1 does a reconstruction of the primary vertex (PV). Hadrons containing a charm or beauty quark have a high mass and usually decay weakly which results in a long flight distance from the PV. Therefore many HLT1 lines contain high transverse momentum (PT) cuts and a separation of the muon's trajectory from the PV. The HLT1 reduces the data rate from 870 kHz to 43 kHz.

With this rate HLT2 can run a full reconstruction of the event combining the detector's data to tracks and particles. Therefore the HLT2 lines are capable of doing selections including specific decays and particles and store the results for further processing. The output is a 3 kHz data rate. [25]

As a drawback of the HLT2's reconstruction speed, its quality in Run I was not sufficient

for further processing. Thus events passing the trigger were reconstructed again but more precisely offline. A single event offline reconstruction needs two seconds, which is about 80 thousand times longer than the HLT2 decision.

Because analysts are not interested in every event, which passed an arbitrary line, a preselection is used to group similar subsamples together. Like the offline reconstruction this so-called *stripping* needs a lot of computation power and is done centrally.

The analyst can now access the stripping's output, which includes the wanted events. Then it is possible to search through the events for the desired specific decay and produce so-called nTuples, which contain the included particle's properties and thus are sufficient for a further physical analysis.

This data flow, which consists of storing the whole event, an offline reconstruction and the stripping, is called 'Full stream'. Its beneficial effect is a very accurate reconstruction, but it has high costs in terms of bandwidth and memory usage.

The Turbo Stream

In Run I the LHC provided a center of mass energy of 7 to 8 GeV which increased up to 13 GeV in Run II. The increase in energy results in a higher multiplicity, thus more data per event was expected. To face the resulting problem of limited bandwidth and memory, the 'Turbo Stream' was implemented. Due to a huge improvement of the online reconstruction, it was then possible to use the online reconstruction directly for the analysis.

The general idea is to use this online reconstruction for a selection inside the trigger. Instead of storing the whole event, only tracks of interest are stored and the rest of the event is rejected. Therefore the needed memory per event is lower, which results in a reduction of the bandwidth. Additionally no offline reconstruction and no stripping is needed. For Run II both methods are used. Since it is important to establish the online trigger, different turbo versions were released during Run II:

Turbo saves the decay tree of the triggered candidate only. Since all the other event data is neglected it is very efficient in terms of bandwidth, but the triggered candidate is often not sufficient for an analysis.

Turbo++ saves the whole event similar to the Full stream. Therefore arbitrary combinatorics can be performed, but the storing of full events still costs a lot of memory. This method is used in Run II for establishing the online reconstruction and is also used in this analysis.

TurboSP, Turbo with selective persistence, is a compromise between Turbo and Turbo++.

Additional to the triggered particle other tracks can be stored. These additional tracks should give enough information for further analysis, but the price in terms of memory and bandwidth is quite low. Thus the TurboSP is the preferred method for Run III and knowledge about its efficiency is indispensable for the upgrade.

In Figure 4.2 the data flow is shown. For every step another application optimized for the specific task is used. For simulations the whole event and detector response is simulated by the Gauss application. The rest of the data flow stays the same as for real data.
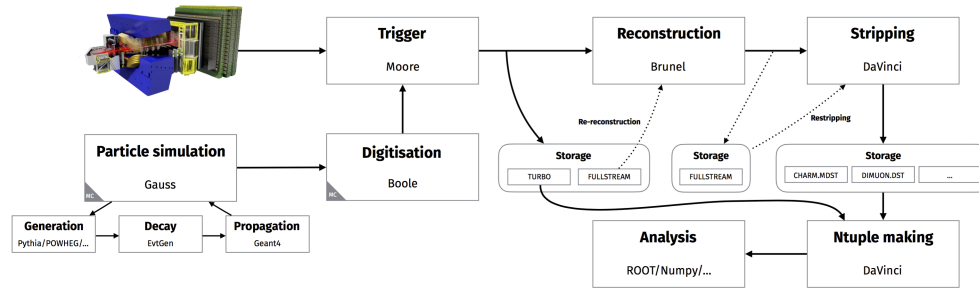
Figure 4.2: The LHCb data flow for the Full stream, Turbo Stream and simulated data taken from [26].

In conclusion, the Turbo Stream can use the HLT2 online reconstruction and thus the output of the trigger directly, whereas a whole computational intensive offline reconstruction and stripping is necessary for the Full stream.
While the Full stream stores every triggered event completely, the Turbo stream (At least the TurboSP) only stores the triggered particles and certain extra tracks to reject data independent of signal. This leads to a huge reduction of bandwidth, which will be far more important regarding Run III, whose multiplicity is ∼ five times higher than in Run II. This motivates the goal to compare the yields of the two streams to verify the functionality of the Turbo stream and its online reconstruction.

Information about the changes for Run III is shown in chapter 7.

5 Analysis for Run 2

5.1 Method

The first step to establish this channel is the measurement of the branching fraction. The branching fraction $\mathcal{B}$ defines the fraction between a particle decaying in a certain decay channel to the total number of those particles, which decay.
For the decay of this analysis, it is given by

$$\mathcal{B}(\Lambda_b^0 \to J/\Psi\Lambda^0\Phi) =$$

$$\frac{N(\Lambda_b^0 \to J/\Psi(\to \mu^+\mu^-)\Lambda^0(\to p\pi^-)\Phi(\to K^+K^-))}{\int \mathcal{L}dt \cdot 2\sigma_{b\bar{b}} \cdot f_{\Lambda_b^0} \cdot \epsilon_{J/\Psi\Lambda^0\Phi} \cdot \mathcal{B}(J/\Psi \to \mu^+\mu^-) \cdot \mathcal{B}(\Lambda^0 \to p\pi^-) \cdot \mathcal{B}(\Phi \to K^+K^-)} \quad (5.1)$$

where $N(\Lambda_b^0 \to J/\Psi(\to \mu^+\mu^-)\Lambda^0(\to p\pi^-)\Phi(\to K^+K^-))$ is the total number of observed events within this channel, $\int \mathcal{L}dt$ the integrated luminosity for the related time period, $\sigma_{b\bar{b}}$ the cross section of $b\bar{b}$, $f_{\Lambda_b^0}$ the probability to form a Λ_b^0 out of a b-quark, $\epsilon_{J/\Psi\Lambda^0\Phi}$ the total efficiency of observing the decay and $\mathcal{B}(J/\Psi \to \mu^+\mu^-), \mathcal{B}(\Lambda^0 \to p\pi^-), \mathcal{B}(\Phi \to K^+K^-)$ the branching fractions of the 3 daughter particles to their final states.

Since the quantities $\int \mathcal{L}dt$, $f_{\Lambda_b^0}$ and $\sigma_{b\bar{b}}$ can only be measured with big uncertainties it is convenient to measure the branching fraction relative to a so-called reference channel. For this analysis the reference channel $\Lambda_b^0 \to J/\Psi\Lambda^0$ is used. This channel is preferred, because using the same modes as in the signal channel many sub branching fractions cancel out and the same trigger lines and stripping can be used, which excludes further systematic uncertainties.

$$\frac{\mathcal{B}(\Lambda_b^0 \to J/\Psi\Lambda^0\Phi)}{\mathcal{B}(\Lambda_b^0 \to J/\Psi\Lambda^0)} = \frac{N_{sig} \cdot \epsilon_{ref}}{N_{ref} \cdot \epsilon_{sig} \cdot \mathcal{B}(\Phi \to K^+K^-)} \quad (5.2)$$

Here sig stands for the signal channel $\Lambda_b^0 \to J/\Psi\Lambda^0\Phi$ and ref for the reference channel $\Lambda_b^0 \to J/\Psi\Lambda^0$.
With the PDG value of $\mathcal{B}(\Phi \to K^+K^-) = 0.489 \pm 0.005$ [17] the branching fraction ratio is an efficiency corrected fraction of the raw yields. The raw yield ratio $\frac{N_{sig}}{N_{ref}}$ is used

to validate the Turbo stream on such a complex decay, involving long living hyperons. Also 2015 MC is used for the Full stream for a first estimation of the branching fraction using Run II data.

5.2 Trigger and Stripping for Run 2

The obtained data is already preselected by the stripping or trigger for Full stream and Turbo stream respectively. To evaluate the resulting data it is important to know, which selection was applied earlier.

5.2.1 Full stream

For the Full stream the nTuples arrive from the stripping. The strippingline used for this channel is *FullDSTDiMuonJpsi2MuMuDetachedLine* version 28r1. This line combines events which are likely to contain a J/Ψ, which decays in two muons. Since only the muons are detected, their tracks are combined with a displaced vertex of the VELO and the mother's properties are calculated. Cuts applied on the reconstructed J/Ψ and its daughters can be found in Table 5.1

Particle	Cut
J/Ψ	m $\in$(2996.916, 3196.016) MeV/c^2 DLS > 3 $\chi^2_{Vertex} < 20$
Muons	PT > 500 MeV/c PIDmu > 0 $\chi^2_{\text{DOCA}} < 30$

Table 5.1: FullDSTDiMuonJpsi2MuMuDetached Stripping Line version 28r1

Here a short description of the used parameters is shown.

m is the *mass.* Due to the reconstruction a four momentum p is assigned to the J/Ψ. The mass is calculated by

$$m = \sqrt{p^2} \tag{5.3}$$

Since we are interested in muons created by a J/Ψ (PDG mass is (3096.916 ± 0.011) Mev/c^2) this loose cut excludes mother particles which are unlikely to be the latter.

DLS stands for *decay length significance* and is a measure for the distance to the primary vertex, which is the pp collision point of the whole decay. This cut ensures that the J/Ψ comes from a long living particle like the Λ_b^0 (flight distance is $\sim 440~\mu m$) and not from the primary vertex directly.

PT is the momentum transversal to the beam.

PIDmu is a measure of the particle identification system for the particle's likelihood to be a muon. therefore the RICH detectors are used and the resulting likelihood L_μ is compared to the likelihood of a pion L_π.

$$\text{PIDmu} = \ln\left(\frac{L_\mu}{L_\pi}\right) \tag{5.4}$$

$\chi^2_{\textbf{DOCA}}$ is a topological requirement. When the vertex is fitted, it requires a maximum *distance of closest approach* to improve the likelihood for the two muons coming from the same vertex.

Since the Λ_b^0 is a long living particle and the event is triggered by a J/Ψ decaying into two muons, this stripping line is the appropriate choice for this analysis.

The stripping line groups together several trigger lines, thus the choice of a trigger decision is applied after the stripping. The advantage of using a certain trigger decision is the knowledge of the decisions, which lead to this data set, which can be used for efficiency calculations later on. Here trigger on signal (TOS) decisions are used. This means that the particles in the signal decay are used for the decisions and not other particles of the event.
The trigger lines used for this analysis are shown in Table 5.2.

The L0MuonDecision (DiMuon) is passed, if the muon detector detects one (two) tracks above a certain PT threshold. HLT1 matches those muon tracks with displaced vertices in the VELO. HLT1TrackMuon requires a maximal χ^2_{track} and a minimal $\chi^2_{IP,PV}$ on a single muon. While χ^2_{track} is a quality check, the *impact parameter* (IP) is a measure for the closest track distance to the primary vertex. The DiMuonHighMass decision requires a certain invariant mass of two muons coming from the same vertex in the VELO. HLT1AllL0 requires track quality for a single muon passing any L0 line. The DiMuonDetachedJpsiDecision's cuts are very similar to the cuts of the stripping.

LO
L0MuonDecision
L0DiMuonDecision
HLT1
Hlt1DiMuonHighMassDecision
Hlt1TrackMuonDecision
Hlt1TrackAllL0Decision
HLT2
Hlt2DiMuonDetachedJPsiDecision

Table 5.2: Trigger lines used for the Full stream selection.

The same stripping and trigger lines are used for signal and reference channel. This leads to canceling of systematic uncertainties related to the stripping and trigger in the yield ratio.

5.2.2 Turbo stream

The Turbo stream data set results of the online reconstruction of the HLT2. Every event passing the *HLT2DiMuonJpsiTurbo* line will be stored. Here the Turbo++ method is used. Turbo++ stores the whole reconstructed event of the HLT2 reconstruction. Therefore it is similar to the Full stream in terms of functionality, but uses the turbo online reconstruction. The selection used in this line is shown in Table 5.3. In comparison to the Full stream a looser cut is applied on χ^2_{vertex} and the mass of the two muons. Additionally no cut on the DLS is used and the cut on the PIDmu variable is stricter. To compare the data to the Full stream the same L0 and HLT1 decisions are used.

Particle	Cut
J/Ψ	m ∈ [2976.916 , 3216.916] MeV/c^2
	$\chi^2_{Vertex} < 25$
	PT > 500 MeV/c
Muon	PIDmu > 1

Table 5.3: DiMuonJpsiTurbo

The output of the turbo HLT2 decision and the stripping respectively is sufficient preselected to allow further processing of the data.

In the next step the triggered J/Ψ is combined with the other daughter particles Λ^0 and Φ (For the reference channel only Λ^0 is added). Further physical and quality cuts are added to clean the signal and reduce background.
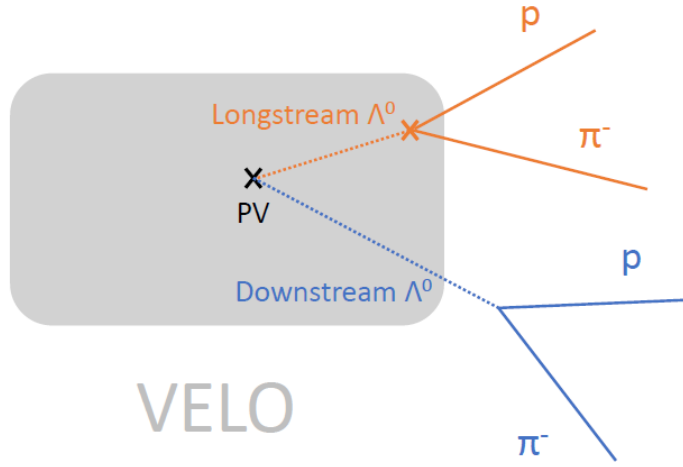
Figure 5.1: The differences between longstream and downstrean are shown for Λ^0. A longstream Λ^0 decays inside the VELO and a downstream Λ downstream of the VELO. For the longstream Λ^0 the vertex position is used for the track reconstruction, while no vertex position is measured for the downstream Λ^0. The dotted lines presents neutral particles and the solid lines charged particles.

5.3 nTuples

Although Turbo++ uses the online reconstruction and the Full stream the offline reconstruction, the same selection for both methods can be used. Since the Λ^0 is a long living particle it is possible, that it decays into p and π^- downstream of the VELO. The differences are visualized in Figure 5.1. Due to different efficiencies the data is analyzed separately for downstream (DD) and longstream (LL) tracks. In the signal channel also a Φ is build of two kaons. All those daughter particles are then combined to Λ_b^0 and the resulting particle properties are stored as nTuples. The used selection for the signal channel is shown in Table 5.4. The construction of the decay, further selections and the fitting model are equivalent to Run I [5]. Due to low statistics in the signal channel it was decided not to tune the cuts further.

$\chi^2_{\mathbf{IP},\mathbf{PV}}$ is a measure for the impact parameter in terms of χ^2 of the fit. The impact parameter is the shortest distance between a track and the primary vertex of the decay and therefore an index whether a particle comes directly from the PV or not.

Particle	Cut
J/Ψ	m $\in$ [3040 , 3150] MeV/c^2
Λ^0	PT > 100 MeV/c
	m $\in$ [1000 , 1220] MeV/c^2
Φ	χ^2_{Vertex} < 12
	m $\in$ [969.445 , 1069.445] MeV/c^2
	PT > 200 MeV/c
Kaons	PT > 100 MeV/c
	$\chi^2_{IP,PV}$ > 10
	$\chi2_{track}/DOF$ < 3
	ProbNN$_{ghost}$ < 0.3
Λ_b^0	m $\in$ [5000 , 7000] MeV/c^2
	χ^2_{Vertex} < 16
	$\chi^2_{IP,PV}$ < 25
	DIRA > 0.999

Table 5.4: Creation of the nTuples

Data	Run II Full stream		Run II Turbo	
Channel	Signal channel	Ref. channel	Signal channel	Ref. channel
Int. Luminosity $[pb^{-1}]$	1645 $\pm$ 33	1644 $\pm$ 33	1646 $\pm$ 29	1645 $\pm$ 29
Number of Candidates	96074	2696329	140142	6307286

Table 5.5: The integrated luminosity and candidates for Run II.

DIRA is the cosine between the angle of the momentum direction and a straight line from the PV vertex to the particle's decay vertex.

ProbNN$_{ghost}$ is the probability for the particle's track to be a ghost. A ghost track is a track, that is obtained by combining hits in the tracking system, which do not belong together.

For the reference channel there is no Φ in the decay, thus the cuts are slightly different. Due to higher statistics a tighter mass cut for the Λ^0 is chosen as m $\in$ [1090, 1150] MeV/c^2. Since no Φ is produced, higher momenta for the other daughters are expected and the Λ^0 PT cut is raised to 500 MeV/c.

As a result four data samples are created, one for each data taking method and channel. The integrated luminosities and number of candidates are shown in Table 5.5.

DecayTree fitter

19

To improve the mass resolution a so-called 'decaytree fitter' (DTF) is used. This kinematic fit constrains the mass of the particles Λ^0 and J/Ψ to the PDG mass and further the Λ_b^0 is constrained to point to the best PV. This influences the kinematics used for the Λ_b^0 properties. A cleaner distribution for the resulting mass is expected, thus the DTF mass is used for the fits.

The spectra of the Λ_b^0 DTF invariant mass distributions for signal and reference channel are shown in Figure 5.2. The PDG Λ_b^0 mass is m $= (5619.5 \pm 0.4)$ MeV/c^2. Due to similar distributions, only the Full stream is shown here. For the reference channel the Λ_b^0 peak is clearly visible on top of an exponential decreasing background. The peak in the signal channel is not visible due to too much background. The different background shape is expected due to different phase space distributions. The mass of the Λ_b^0 candidates is calculated with the energies and momenta of their daughter particles. Therefore the sum of the daughter's masses introduces a lower boundary to the mass of the Λ_b candidates. For the reference channel a J/Ψ and a Λ are combined. The resulting boundary for the Λ_b^0 mass is at ~ 4200 MeV/c^2, so that the expected decreasing exponential distribution occurs.

For the signal channel an additional Φ occurs in the decay, which introduces a lower boundary to the Λ_b^0 invariant mass at approximately 5200 MeV/c^2. The presence of this close boundary for the Λ_b^0 candidates results in a different distribution, which is still increasing at the expected Λ_b^0 invariant mass.
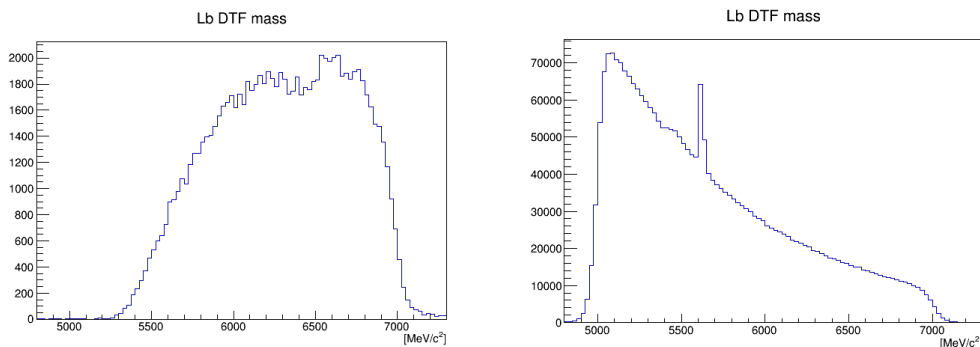
Figure 5.2: The DTF spectra for the Full stream Λ_b^0 invariant mass for the signal (left) and reference (right) channel. The Λ_b^0 peak is clearly visible in the reference channel, while it is not visible in the signal channel, because of too much background.

Particle	Cut
Λ_b^0	PT $\in$[0, 20000] MeV/c
	$\eta \in$[2.2, 4.5]
Λ^0	FD > 1
	m $\in$[1108, 1124] MeV/c^2 (DD)
	m $\in$[1112, 1120] MeV/c^2 (LL)
Φ	m $\in$[1005, 1035] MeV/c^2
Kaons	P $\in$[5000,60000] MeV/c
	$\eta \in$[2, 4.9]
J/Ψ	m $\in$[3040,3160] MeV/c^2

Table 5.6: Further cuts to clean the signal peak. Mass cuts are applied on the daughter particles.

5.4 Preselection

For the fits additional cuts are used to reduce further background on the Λ_b^0 invariant DTF mass. The most important cuts are shown in Table 5.6. Additional to further cuts on momenta, cuts on the *pseudorapidity* η and the flight distance FD are applied. The momentum cut on the kaons is used, because the particle identification system only works well in this momentum range. The η cuts reflect the detector's geometrical acceptance, which covers a range of $\eta \in$[2,5].

The pseudorapidity is a spatial coordinate describing the angle Θ to the beam axis.

$$\eta = -\ln[\tan\left(\frac{\Theta}{2}\right)] \tag{5.5}$$

Tight mass cuts are applied on the added daughter particle Λ^0 and Φ. Since the peak in the mass spectra are of interest, the sidebands are excluded. The mass spectra of the daughters in the signal and reference channel with cuts depicted are shown in Figure 5.3.

For the reference channel the same cut for Λ^0 is used.

5.5 Fit model

The resulting data is fitted using following model:

For the signal peak a double-Gaussian is used. The Gaussian distribution is defined as

$$G(x|\mu,\sigma) = \frac{1}{\sqrt{2\pi\sigma^2}} \exp\left(\frac{(x-\mu)^2}{2\cdot\sigma^2}\right) \tag{5.6}$$
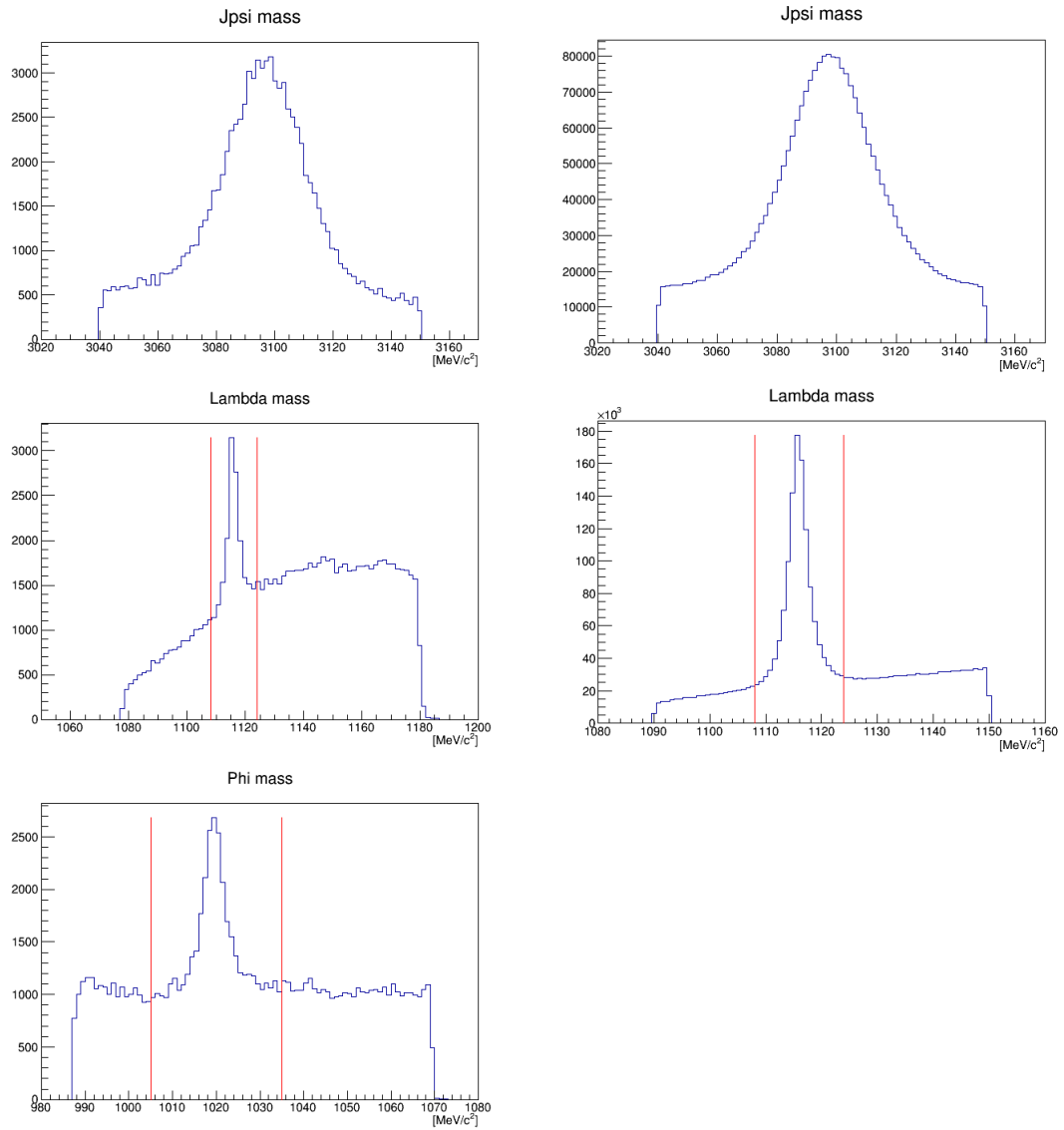
Figure 5.3: The mass spectra of the signal channel (left) and reference channel(right) with depicted cuts. The mass window between the red lines is used for the fit on the Λ_b^0 mass. From top to bottom the spectra for the J/Ψ, Λ^0 and Φ are shown. No mass cut on the J/Ψ is applied.

22

with the mean μ and the standard deviation σ. The double-Gaussian is a normalized sum of two Gaussians. Thus the signal probability density function S is described by the following model.

$$S(x|f, \mu, \sigma_1, \sigma_2) = f \cdot G(x|\mu, \sigma_1) + (1 - f) \cdot G(x|\mu, \sigma_2) \tag{5.7}$$

with the fraction $f \in [0, 1]$.

The background is modulated by an exponential distribution B

$$B(x|cbg) = A \exp(x \cdot cbg) \tag{5.8}$$

with A being the normalization. As shown for the total distributions in the Λ_b^0 invariant mass, a decreasing background is expected for the reference channel and an increasing one for the signal channel, therefore the factor *cbg* is constrained to be negative or positive respectively. The resulting total model P can now be described as

$$P(x) = N_{Sig} \cdot S(x|f, \mu, \sigma_1, \sigma_2) + N_{bckg} \cdot B(x|cbg) \tag{5.9}$$

5.5.1 Monte Carlo Simulation

For precise physical measurements, it is important to entangle physical phenomena and detector effects. Simulations of data, so-called *Monte Carlo Simulations* (MC) is used to account for detector effects, which influence the real data. For example the data is influenced by the detector's finite resolution or imperfections in the reconstruction can occur. Since the physical behaviour of MC is know, it is used to reveal those detector effects and to take those into account for real data.

In this analysis 2011 and 2012 MC of the signal and reference channel is used to determine the signal shape. By studying the MC, the double-Gaussian distribution S was chosen. The parameters of the shape f, μ, σ_1 and σ_2 are taken from MC and applied on data. Additionally 2015 MC is used in the next chapter for a first efficiency correction of Run II data within these channels.

6 Fits and results for Run 2

Using the selection described in chapter 5 and the described model for the probability distribution function, the obtained fitresults are used for the yield ratio. The MC fits for the DD and LL sample are shown in Figure 6.1. The number of events per two MeV is shown in a mass window of 5580 MeV/c^2 to 5660 MeV/c^2 for the signal channel and in a mass window of 5520 MeV/c^2 to 5720 MeV/c^2 for the reference channel. The broader window in the reference channel is used, because of higher statistics and a broader peak. Below the mass distributions, the pulls are shown. The peak is clearly visible at 5620 MeV/c^2. Since no background is simulated in the MC, only the signal is fitted.
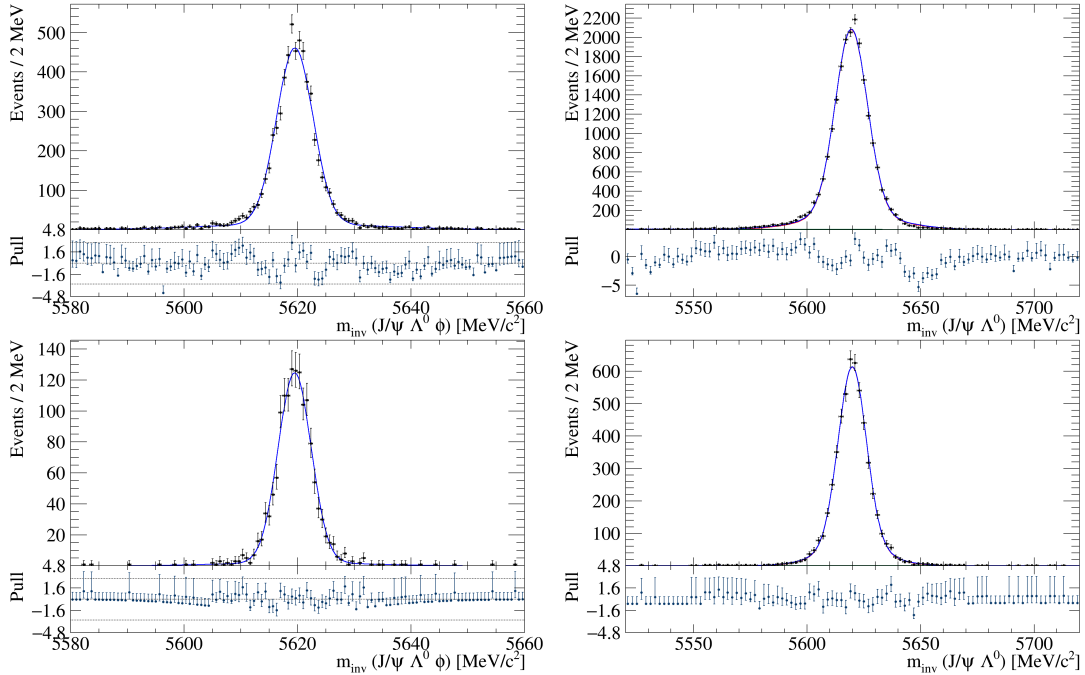
Figure 6.1: Fits of the Run I MC data for signal (left) and reference (right) channel. The fits are separately done for the DD (top) and LL (bottom) sample. The resulting shape is used for the fit on real data.

The different fits for the Full stream and Turbo stream, using the shape of the Run I MC, are shown in Figure 6.2 and 6.3. The total distribution is shown in blue, the

Data	Run II Full stream		Run II Turbo	
Channel	Signal channel	Ref. channel	Signal channel	Ref. channel
N_{sig}	42 ± 8	16800 ± 200	43 ± 8	16600 ± 200
N_{bckg}	67 ± 9	59300 ± 300	91 ± 11	75000 ± 300

Table 6.1: Yields of the DD sample for run2 for Full stream and Turbo stream.

background in green and the extracted signal distribution in red. The peaks are clearly visible in the reference channel. For the signal channel there is only low statistics, which results in high uncertainties. Due to too low statistics in the longstream (LL) subset only the DD sample is used for further analysis. The yields of the DD sample are shown in Table 6.1.
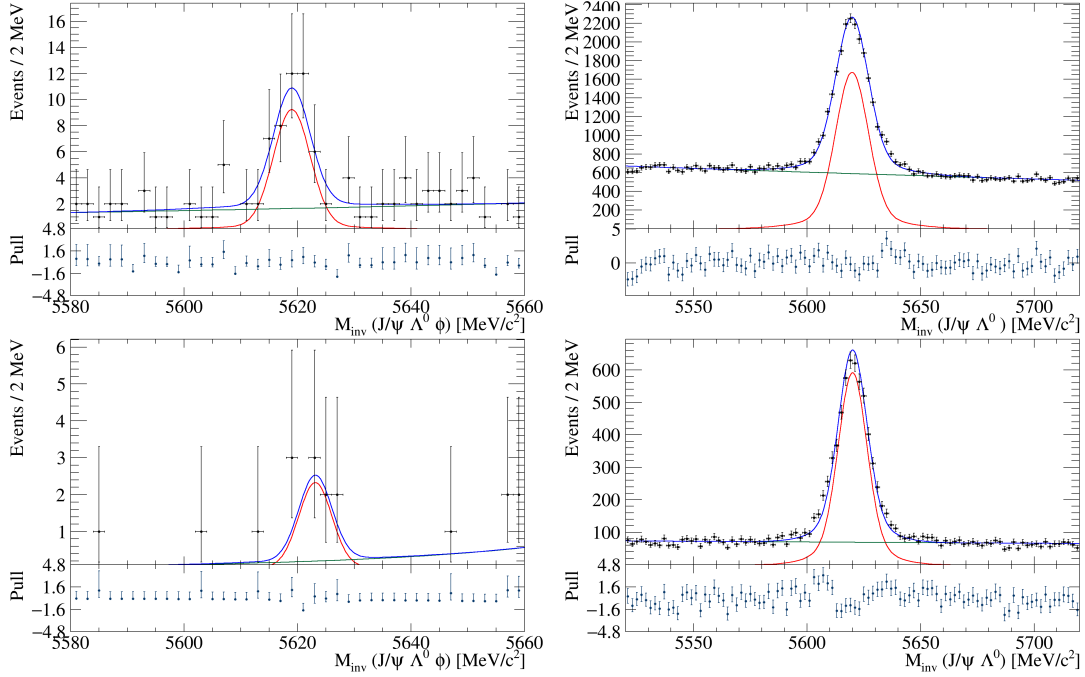
Figure 6.2: Fits of the Run II Full stream data for signal (left) and reference (right) channel. The fits are separately done for the DD (top) and LL (bottom) data sample.

Mass resolution

The fits are repeated without fixing the standard deviation on MC to compare the mass resolution of turbo and full stream. Due to higher statistics, the reference channel is used. The standard deviations are shown in Table 6.2. For both Gaussians the standard
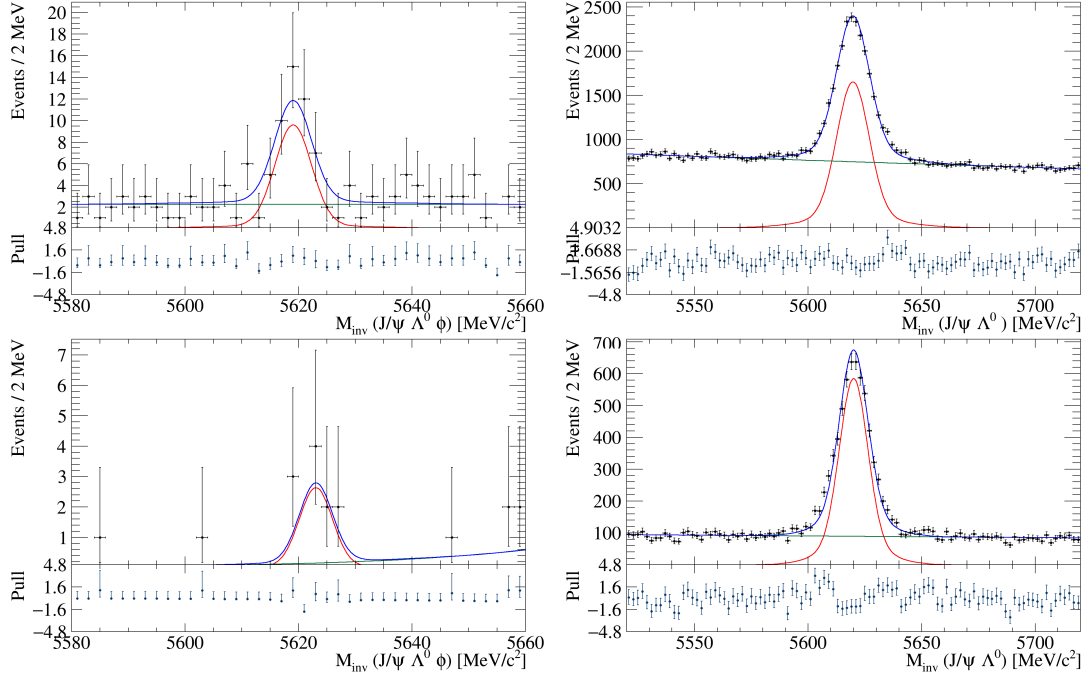
Figure 6.3: Fits of the Run II turbos data for signal (left) and reference (right) channel. The fits are separately done for the DD (top) and LL (bottom) data sample.

channel	σ_1 [MeV/c^2]	σ_2 [MeV/c^2]
Full stream	9.4 ± 0.2	4.6 ± 0.2
Turbo stream	9.3 ± 0.2	4.7 ± 0.2

Table 6.2: The standard deviations of the reference channel for Turbo stream and Full stream respectively.

deviations are consistent within the 1 σ interval, which validates the use of the Turbo stream and its online reconstruction.

Fits for Run I

The yields for Run I can be reproduced by the same selection as for Run II. Using 2011 and 2012 data the fits are shown in Figure 6.4 and the resulting yields and integrated luminosity in Table 6.3.
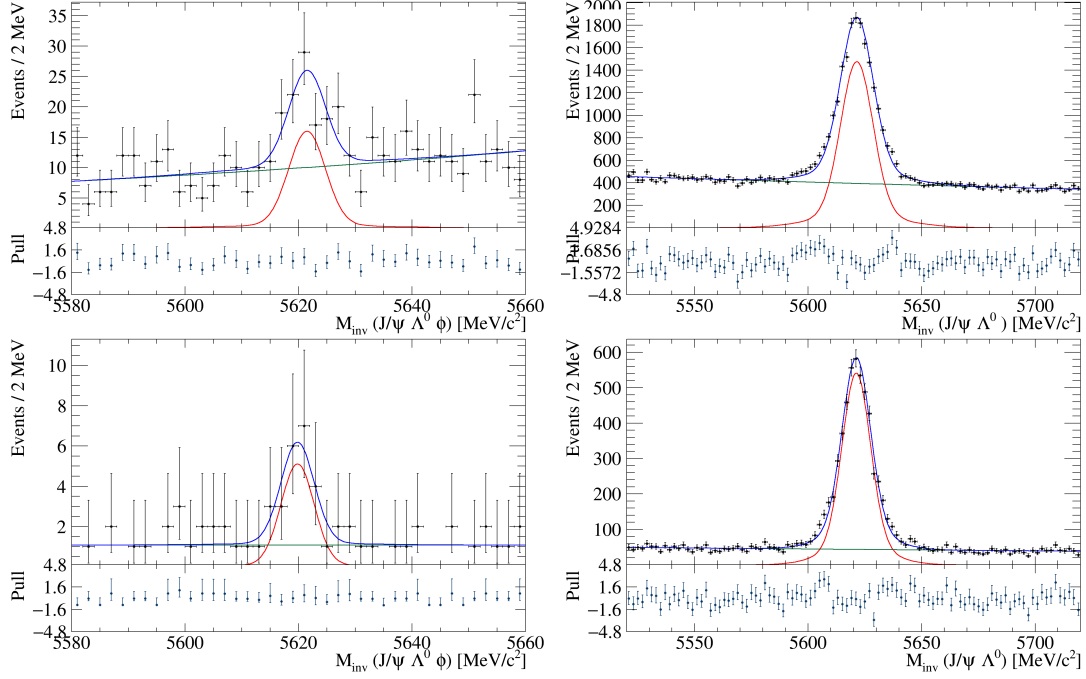
Figure 6.4: Fits of the Run I data for signal (left) and reference (right) channel. The fits are separately done for the DD (top) and LL (bottom) sample.

Data	Run I Full stream	
Channel	Signal channel	Ref. channel
N_{sig}	72 ± 13	14830 ± 160
N_{bckg}	402 ± 23	39700 ± 200
Int. luminosity	2956 ± 1	2815 ± 1

Table 6.3: Yields for run1.

6.1 Results for Run 2 and comparison to Run 1

With the fitresults in Table 6.1 the ratio between signal and reference channel for both data taking methods for Run II can be calculated:

$$\text{Run II Full stream} : \frac{N_{sig}}{N_{ref}} = 0.0025 \pm 0.0005$$

27

$$\text{Run II Turbo stream}: \frac{N_{sig}}{N_{ref}} = 0.0026 \pm 0.0005$$

The results are consistent within the 1 σ interval, which shows, that the Turbo stream and its online reconstruction are capable of selecting and storing as many candidates as the Full stream. In comparison of the background yields, the background level of the Turbo stream is 27 % higher.

Since the raw yield ratio is observed, the results for Run I are reproduced without efficiency correction to make the results comparable. Including Table 6.3, the yield ratio is found to be

$$\text{Run I}: \frac{N_{sig}}{N_{ref}} = 0.0049 \pm 0.0009,$$

which is approximately twice as high as for Run II. Since the branching fraction is independent of the runs, the efficiency correction $\frac{\epsilon_{ref}}{\epsilon_{sig}}$ is expected to be higher than in Run I.

6.2 Run 2 efficiency correction

For an estimation of the efficiencies of the Full stream for 2016 data, 2015 MC is used. Since the detector for 2015 and 2016 is the same, the efficiencies are expected to be similar which justifies the use of 2015 MC for 2016 data. The same workflow as for the real data is used, but in contrast to the 2016 data, the total number of events passing the L0 trigger is known. Since the L0muon trigger is very efficient and the efficiency will cancel out in the ratio used for the efficiency correction, it is neglected for the efficiency calculation in this thesis. Including the total number of MC candidates N_{tot} and the resulting signal yields N_{sig} we get the total efficiency ϵ_{tot}.

$$\epsilon_{tot} = \frac{N_{sig}}{N_{tot}} \tag{6.1}$$

The fits on the whole MC sample of the signal and reference channel are shown in Figure 6.5.
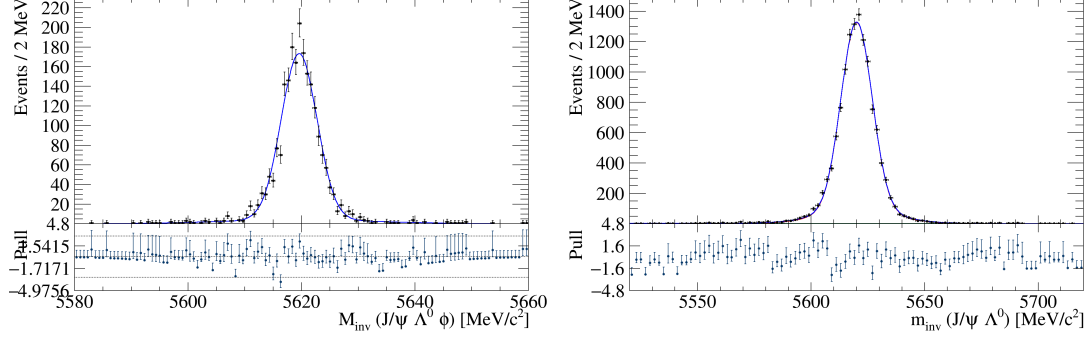
Figure 6.5: Fits of the 2015 MC for signal (left) and reference (right) channel.

6.2.1 PT correction

In Figure 6.6 the Λ_b^0 PT distributions are shown for MC and data. The MC PT distributions do not show the correct shape of the data, which also occurred in Run I [5], due to too less knowledge of the Λ_b^0 behavior for the simulation. Since this has a huge impact on the resulting yields, a reweighting is used. Therefore the PT distribution is binned into n bins for real and MC data respectively. Due to higher statistics the reference channel is used, but it was shown in the Run I analysis, that the resulting weights can be applied on both channels. The ratio between data and MC is used to calculate the weights w_i for each bin i.

$$w_i(PT) = \frac{N_{data,i}}{N_{MC,i}} \cdot \frac{N_{MC,tot}}{N_{data,tot}} \tag{6.2}$$

With X as either MC or data $N_{X,i}$ is the respect number of entries in bin i and $N_{X,tot}$ the total number of entries in the histogram. The weights are chosen such that the PT shape equals the one of the data, but the total number of entries after reweighting stays the same.

$$\sum_{i=1}^{n} w_i \cdot N_{MC,i} = N_{MC,tot} \tag{6.3}$$

The weighted distribution for the MC of the reference channel is shown in Figure 6.7. For the correction the weighted yields N_{Weight} and unweighted yields $N_{NoWeight}$ are important. Instead of a fit, every entry inside the mass window of [5590,5650] MeV/c^2 is counted. For the unweighted yields $N_{NoWeight}$ every entry counts as one, while every entry counts as the corresponding weight of its PT for the weighted yields N_{Weight}.

$$N_{NoWeight} = \sum_{j = \text{Entries in interval}} 1 \tag{6.4}$$

29
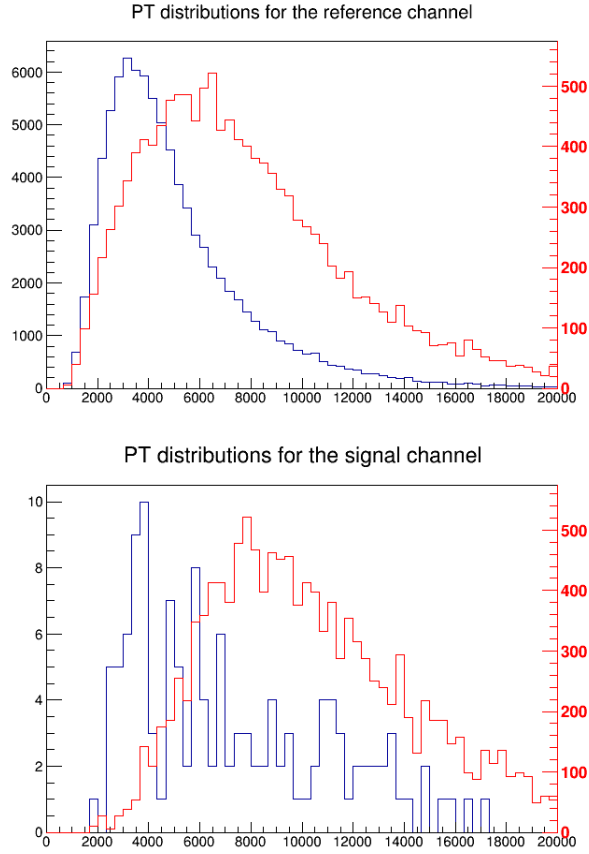
Figure 6.6: The PT distributions for the reference channel(top) and signal channel (bottom). The MC distribution is shown in red and the data distribution in blue.

$$N_{Weight} = \sum_{\text{j = Entries in interval}} w(PT_j) \tag{6.5}$$

The weighted and unweighted yields are used for a correction ϵ_{corr} of the MC yields.

$$\epsilon_{corr} = \frac{N_{Weight}}{N_{NoWeight}} \tag{6.6}$$

The yields and corrections for signal and reference channel respectively are shown in Table 6.4 and the resulting MC yields and the efficiency corrections ϵ_{tot} are shown in Table 6.5.

30
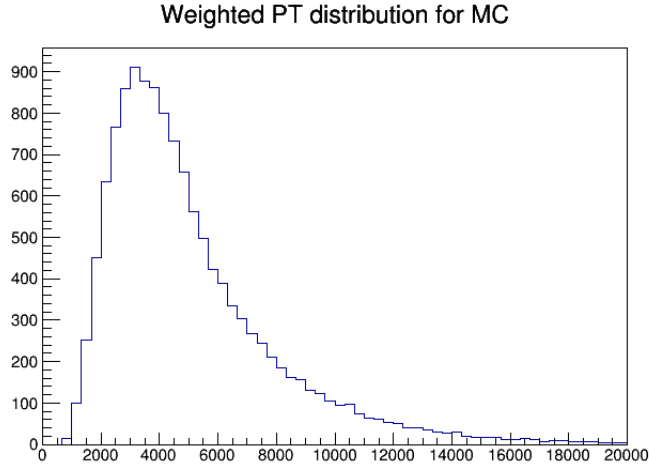
Figure 6.7: The weighted PT distribution for the MC of the reference channel. The total number of events stays the same, while the shape changes to the one of the real data.

Data	2015 MC	
Channel	Signal channel	Ref. channel
N_{Weight}	1121	12367
$N_{NoWeight}$	2227	12425
ϵ_{corr}	0.503	0.995

Table 6.4: The fitresults for 2015 MC and the resulting efficiency.

6.3 Branching fraction ratio for Run 2

With the yields on real data and the efficiency corrections, the branching fraction can be calculated for each channel with Equation 5.2. In terms of variables used in this analysis the branching fraction ratio can be calculated by

$$\frac{\mathcal{B}(\Lambda_b^0 \to J/\Psi\Lambda^0\Phi)}{\mathcal{B}(\Lambda_b^0 \to J/\Psi\Lambda^0)} = \frac{N_{sig} \cdot \epsilon_{tot,ref}}{N_{ref} \cdot \epsilon_{tot,sig} \cdot \mathcal{B}(\Phi \to K^+K^-)} \tag{6.7}$$

with the indices ref and sig for the reference channel and signal channel respectively. The resulting branching fraction ratio is found to be

$$\frac{\mathcal{B}(\Lambda_b^0 \to J/\Psi\Lambda^0\Phi)}{\mathcal{B}(\Lambda_b^0 \to J/\Psi\Lambda^0)} = (5.9 \pm 1.1)\%. \tag{6.8}$$

Data	2015 MC	
Channel	Signal channel	Ref. channel
N_{sig}	2221 $\pm$ 47	12484 $\pm$ 115
$\epsilon_{corr} \cdot N_{sig}$	1117 $\pm$ 24	12422 $\pm$ 114
N_{tot}	310658	299465
ϵ_{tot}	0.0036 $\pm$ 0.0001	0.0415 $\pm$ 0.0004

Table 6.5: The fitresults for 2015 MC and the resulting efficiency.

7 Upgrade studies for Run 3

The LHC will shut down in the end of 2018. The following time will be used to upgrade the detector and prepare Run III.

For Run III LHCb is going to increase the luminosity to $2 \cdot 10^{33}$ cm^{-2}s^{-1} [27]. While the number of primary vertices per event was kept constant at approximately 1 for Run I and Run II, the higher luminosity results in ~ 5 pp collisions per event and thus a five times higher multiplicity for Run III. Additionally the L0 hardware trigger will be removed, so the input rate for the HLT1 trigger will increase from 1 MHz to an effective rate of 30 MHz. The increased multiplicity and increased input rate will result in a huge increase of needed bandwidth. Since most of the data will be independent of signal, TurboSP will be used to limit the bandwidth. Since it only stores certain tracks, tracks independent of signal can be rejected efficiently. The main reduction of bandwidth will be the rejection of data coming from primary vertices, which do not result in a single positive trigger decision.

The downside of the TurboSP is, that it is not possible to access the rejected tracks offline anymore. Thus it is very important to make sure, that every wanted track is recorded and stored. Therefore the challenge is to minimize memory usage by rejecting as much background as possible, while storing all wanted tracks effectively.

In the so-called *inclusive lines* additional tracks of common particles like Λ^0, π or kaons coming from the same vertex are added to the triggered particle. Since many decays contain similar endparticles, the extra tracks can be used for a huge variety of decays. Storing all the tracks only once and specifying the decay afterwards results in a very efficient memory usage and effective method for Run III.

To tune the selections of the triggered particle and those extra tracks, upgrade MC is available for the different decays. The data is already preselected and only events passing the HLT1 are used for further analysis. An emulation of the HLT2 for Run III is used which is supposed to give reasonable results.

In this analysis the simulated data for $\Lambda_b^0 \to J/\Psi\Lambda^0\Phi$, $\Lambda_b^0 \to J/\Psi\Lambda^0$ and $\Xi_b^- \to J/\Psi\Lambda^0 K^-$ is used. These three decays have similar endparticle, containing Λ, J/Ψ and kaons, thus the aim is to reconstruct these different decays using the same TurboSP
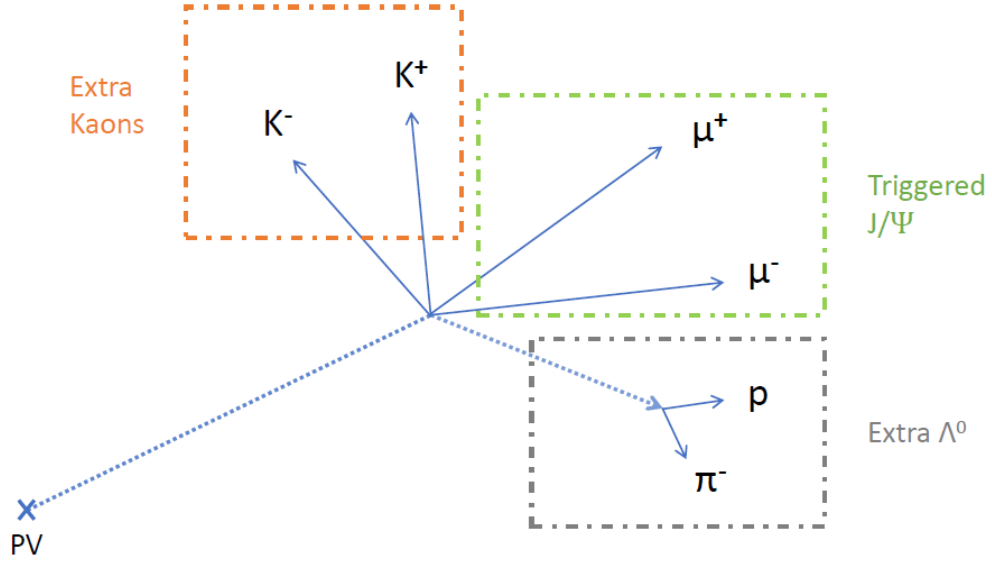
Figure 7.1: The functionality of TurboSP. The dotted lines represent neutral particle which are not visible in the detectors. Note that the Ξ_b^- is charged, so for that MC the track from the PV is a solid line, which represents charged particles.

line, including a J/Ψ trigger and additional kaon and Λ tracks, which come from the same vertex as the J/Ψ. The decay of interest is constructed afterwards using the output of the HLT2 Turbo line similar to Run I and II.

Additional to the MC data a set of random generated events is investigated. Testing the selection on this so-called *MinBias* data is a check, if the selection is strict enough. Since the MinBias sample contains no signal events, the efficiency is expected to be approximately zero. The idea of the TurboSP is shown in Figure 7.1. The existence of J/Ψ is sufficient to pass the trigger. All Λ_0 and kaons of the same vertex are stored additionally. The rest of the event is rejected.

Since the TurboSP J/Ψ trigger should work like the Turbo++ the selection used for the emulation of the HLT2 is similiar to the HLT2JpsiTurbo line used for Run II. The selection for the J/Ψ and extra tracks is shown in Table 7.1.

Additionally to the signal, background is also simulated in the MC data. To reduce passing background additional cuts like the $ProbNNmu$ and $ProbNN_{ghost}$ are used. In comparison to HLT2JpsiTurbo the PT cuts are loosened and no PIDmu cut is applied.

	Trigger emulator J/Ψ	+Λ tracks	+ Kaon tracks
DaughterCut	PT > 0 $\chi^2_{TRACK} < 5$ ProbNN$_{\text{ghost}}$ < 0.4 ProbNNmu > 0.1 $\chi^2_{DOCA} < 30$	PT > 100 m $\in$[1000,1220]	
Mother Cut	$\chi^2_{vertex}/DOF < 25$ |m - $m_{J/\Psi}$| < 120	$\chi^2_{vertex}/DOF < 25$	$\chi^2_{vertex}/DOF < 25$

Table 7.1: Emulation of the J/Ψ turbo SP line for Run III. Units for masses and momenta are MeV/c^2 and MeV/c respectively.

Particle	Cut
Λ_b or Ξ_b	m $\in$[5000,7000] MeV/c^2 $\chi^2_{vertex}/DOF < 16$ DIRA > 0.99
Φ	m $\in$[969.445,1069.445] MeV/c^2 $\chi^2_{vertex}/DOF < 16$

Table 7.2: The cuts used for the reconstruction.

The selection's output is further processed to build the corresponding decay trees and mother particles. In Table 7.2 the additional cuts are shown. A certain fit quality is required using χ^2_{vertex} and DIRA cuts. Furthermore loose mass cuts are used for the Λ_b^0 (m = (5619.5 ± 0.4) MeV/c^2) and Ξ_b^- (m = (5794.9 ± 0.9) MeV/c^2) masses. Since both masses are in the used interval, the same cut is applied. The same mass cut as in Run II is used for Φ.

The resulting number of passed events and possible candidates for every processing step in the emulation and reconstruction are shown in Table 7.3.

The trigger efficiency $\left(\frac{\text{triggered } J/\Psi \text{ events}}{\text{total events}} \right)$ is approximately 48 - 50 % for each sample. Further candidates are lost in the Λ^0 reconstruction. Most of the Λ^0 decay downstream of the VELO. No hits in the VELO means a reduced quality of the proton and pion tracks, which results in a low Λ^0 reconstruction efficiency and a reduction of the passing events to $\sim$ 30 % of the total events.

For $\Lambda_b^0 \to J/\Psi\Lambda^0$ 17.5 % of the events pass the selection. The main inefficiency after the trigger of the J/Ψ is the Λ^0 reconstruction. 2730 candidates were found in 717 events.

MC	$\Lambda_b^0 \to J/\Psi\Lambda^0\Phi$		$\Lambda_b^0 \to J/\Psi\Lambda^0$		$\Xi_b^- \to J/\Psi\Lambda^0 K^-$	
Selection	events	candidates	events	candidates	events	candidates
total events	4117		4088		4477	
triggered J/Ψ	2000	4044	1973	3996	2217	4500
+ Λ^0	1248	3435	1197	3338	1337	3427
+ Kaons	1838	5241	1152	2947	1870	4474
offline reconstruction						
Φ	494	1304				
Λ_b^0 or Ξ_b^-	386	4984	717	2730	795	5252
total efficiency	0.094		0.175		0.178	

Table 7.3: Number of passed events and candidates for every step in the emulation and reconstruction.

For $\Xi_b^- \to J/\Psi\Lambda^0 K^-$ one Kaon track is additionally added to $J/\Psi\Lambda^0$. Due to many added kaons and a flexible Λ^0 fit, many combinations of the daughter particle are accepted, which results in 5252 candidates in 795 events. The total event efficiency is 17.8 %.

For $\Lambda_b^0 \to J/\Psi\Lambda^0\Phi$ the Φ is reconstructed of two different charged kaon tracks. This is possible, because the Φ's flight distance is so short, that its daughter kaons fulfill the quality criteria to be stored as kaons coming form the J/Ψ vertex. Due to many combinatorical possibilities 4984 candidates are found in 386 events, which results in an efficiency of 9.4 %.

For the MinBias sample 170196 events with random tracks were investigated. With 38 event passing the trigger, the resulting trigger efficiency is $\sim$ 0.022 %.

7.1 Rates

With the efficiencies on signal and MinBias MC the trigger's output rates can be estimated.

Signal: The signal rate R_{sig} for $\Lambda_b^0 \to J/\Psi\Lambda^0$ is estimated with the following equation.

$$R_{sig} = \mathcal{L} \cdot \sigma(pp \to \Lambda_b^0 X) \cdot \mathcal{B}(\Lambda_b^0 \to J/\Psi\Lambda^0) \cdot \mathcal{B}(J/\Psi \to \mu^+\mu^-) \cdot \epsilon_{sig} \qquad (7.1)$$

$\mathcal{L}$ is the luminosity which will be $2 \cdot 10^{33}$ cm^{-2}s^{-1} for Run III [27]. The cross section $\sigma(pp \to \Lambda_b^0 X)$ times the branching fraction $\mathcal{B}(\Lambda_b^0 \to J/\Psi\Lambda^0)$ is known for 7 TeV as $\sim$

7 nb [28] and is expected to be twice as high for Run III with a center of mass energy of ~ 14 TeV [29] [30]. The resulting factor $\sigma(pp \to \Lambda_b^0 X) \cdot \mathcal{B}(\Lambda_b^0 \to J/\Psi\Lambda^0)$ is therefore ~ 14 nb. The branching fraction $\mathcal{B}(J/\Psi \to \mu^+\mu^-)$ is known as approximately 0.06 and the efficiency ϵ_{sig} is taken from Table 6.5 as 17.5 %.

The resulting rate is $R_{sig} \sim 0.3$ Hz.

Background: For the background rate R_{bkg} the input rate R_{in} of the HLT1 is used, which will be 30 MHz for Run III. The HLT1 filter efficiency ϵ_{HLT1} is calculated with the total number of MC events produced N_{tot} and the number of MC events, which passed the HLT1 filter N_{HLT1}.

$$\epsilon_{HLT1} = \frac{N_{HLT1}}{N_{tot}} = \frac{2810567}{53993474} = 5.21\% \tag{7.2}$$

The HLT2 efficiency ϵ_{HLT2} of the inclusive line is calculated in the previous section as 0.022 % on the MinBias sample, which simulates the background. The resulting output rate is 344 Hz.

$$R_{bkg} = R_{in} \cdot \epsilon_{HLT1} \cdot \epsilon_{HLT2} = 344\text{Hz} \tag{7.3}$$

7.2 Exclusive lines

Another idea for the trigger lines are exclusive lines, where every line only stores one decay channel. Therefore all cuts shown in Table 7.2 are added to the trigger cuts in Table 7.1 for the respect exclusive trigger line. Since the extra tracks are no longer added to the J/Ψ before combining all daughter particles to the mother particle, the extra track's χ_{vertex}^2/DOF cuts are not applied. This results in slightly higher results than the inclusive line for $\Lambda_b^0 \to J/\Psi\Lambda^0\Phi$ and $\Xi_b^- \to J/\Psi\Lambda^0 K^-$, where more than one particle is added to the J/Ψ. For $\Lambda_b^0 \to J/\Psi\Lambda^0\Phi$ the efficiency is 11.1 % and for $\Xi_b^- \to J/\Psi\Lambda^0 K^-$ 18.0 %. For $\Lambda_b^0 \to J/\Psi\Lambda^0$ the efficiency stays the same.

The huge advantage of exclusive lines is, that the whole decay tree is needed for a positive trigger decision, which excludes far more background than the J/Ψ trigger used for the inclusive line. Running over 170196 MinBias events, the exclusive lines store 5, 10 and 11 events for $\Lambda_b^0 \to J/\Psi\Lambda^0\Phi, \Lambda_b^0 \to J/\Psi\Lambda^0$ and $\Xi_b^- \to J/\Psi\Lambda^0 K^-$ respectively, which results in an efficiency of 0.003 %, 0.006 % and 0.007 %. Therefore including Equation 7.3 the background rate is reduced to 47 Hz, 94 Hz and 109 Hz respectively.

So the exclusive lines are far more efficient in terms of selection and storage usage,

because they reject three to seven times more background. On the other hand the inclusive line is capable of storing data for more than one decay channel. Thus the background rate per decay channel depends on the number of channels, which can be triggered by that line. Another advantage of the inclusive line is, that this method stores the tracks independently of the decay, so the output can be analysed a posteriori for new channels.

8 Conclusion

The first goal of this thesis was to measure the 2016 data yields of the signal channel $\Lambda_b^0 \to J/\Psi\Lambda^0\Phi$ and reference channel $\Lambda_b^0 \to J/\Psi\Lambda^0$ for the two data taking methods *Full stream* and *turbo++* respectively.

The Full stream uses a fast online reconstruction and a more precise one offline, which stores the whole event. Similar events are grouped together in the *stripping*, whose output can be accessed to look for the wanted decay.

The Turbo++ uses a more precise online reconstruction which is sufficient for further analysis, thus no offline reconstruction is needed. Like for the Full stream, the whole event is stored. The analyst can access the output of that turbo line, which contains all information needed for further investigation, so no stripping is required.

Since the Turbo stream is more efficient in terms of memory usage and bandwidth, which will be the limiting factor in data storage for Run III, it is the preferred data taking method for the upgrade. The Turbo stream uses a looser selection which results in more candidates for 2016. The selection, which is equivalent to Run I is applied on both methods and is sufficient to reduce the background to a level, where a mass fit can be applied on the Λ_b^0. The resulting yields are used to calculate the ratio $\frac{N_{sig}}{N_{ref}}$. For the anaylsis the data sample is split into the LL and DD subset. In the LL subset the vertex of the Lambda is in the VELO, for the DD subset downstream of the VELO. Since different efficiency corrections are used for both incidents, they are split up. Not enough statistics for the LL sample is observed, thus only the yields for the DD sample are used for the ratio. The resulting ratios are

$$\text{Run II Full stream}: \frac{N_{sig}}{N_{ref}} = 0.0025 \pm 0.0005$$

$$\text{Run II Turbo stream}: \frac{N_{sig}}{N_{ref}} = 0.0026 \pm 0.0005.$$

The resulting ratios are consistent within the 1 σ interval. The high uncertainties result of the fit on the signal channel. To improve the fit, more statistics is needed.

This is a validation of the Turbo stream on a complex decay topology, involving long living hyperons.

The ratios show, that the Turbo stream and especially the online reconstruction is effective and capable of replacing the Full stream method in the future.

The results of Run I without efficiency correction were reproduced, so they can be compared to Run II.

$$\text{Run 1}: \frac{N_{sig}}{N_{ref}} = 0.0049 \pm 0.0009$$

The raw yield ratio is nearly twice as high for Run I than for Run II. Since the branching fraction is independent of the different runs, the efficiency correction is expected to be ~ 2 times the one of Run I.

For verification 2015 MC is used to estimate the efficiency correction for the Full stream. Since there were no changes in the detector between 2015 and 2016, it is expected, that the 2015 MC gives reasonable results for the efficiencies of 2016. Additionally, a reweighting in the Λ_b^0 PT distribution is used, which results in a factor of ~ 2 in the efficiency correction. The efficiencies are $\epsilon_{sig} = 0.0036 \pm 0.0001$ and $\epsilon_{ref} = 0.0415 \pm 0.0004$. In comparison to the measured efficiencies of Run I, $\epsilon_{sig} = 0.0027$ and $\epsilon_{ref} = 0.024$, the signal channel efficiency increased by 33 % and the reference efficiency by 75%. The resulting ratio explains the huge difference of a factor of ~ 2 in the raw yields. The resulting efficiency corrected branching fraction is found to be

$$\frac{\mathcal{B}(\Lambda_b^0 \to J/\Psi\Lambda^0\Phi)}{\mathcal{B}(\Lambda_b^0 \to J/\Psi\Lambda^0)} = (5.9 \pm 1.1)\%.$$

In Run I the branching fraction was measured as $(5.3 \pm 0.7)\%$ which is in good agreement with Run II (1 σ interval).

In a follow-up analysis the data for 2017 could be added to improve the statistics to reduce statistical uncertainties and to reinclude the LL sample. Including also 2016 and 2017 MC an efficiency correction of the Run II yields would result in a more precise branching fraction measurement, which can be compared to Run I. Also a combination of both runs can be used for a huge improvement in the statistics.

For Run III the TurboSP method will be used. In contrast to Turbo++ only the triggered particle and certain extra tracks are stored by a trigger line, which will further reduce the memory usage. As a disadvantage the neglected tracks and particles are not accessible anymore, wherefore the Turbo++ was used primarily for Run II to implement and test the Turbo method. Since the yield ratio shows, that the turbo selection is similar effective as the Full stream, the next step and last goal of this thesis is to use this knowledge to build the selection for TurboSP. The upgrade MC data for $\Lambda_b^0 \to J/\Psi\Lambda^0\Phi$, $\Lambda_b^0 \to J/\Psi\Lambda^0$ and $\Xi_b^- \to J/\Psi\Lambda^0 K^-$ was used for the trigger line. Due to similar endparticle, all those decays can be reconstructed with a J/Ψ trigger and added Λ^0 and kaons. For the trigger a similar selection to the *HLT2JpsiTurbo* is used.

The total efficiency is 17.5 % for $\Lambda_b^0 \to J/\Psi\Lambda^0$, 17.8 % for $\Xi_b^- \to J/\Psi\Lambda^0 K^-$, 9.4 % for $\Lambda_b^0 \to J/\Psi\Lambda^0\Phi$ and 0.022 % on simulated background. This results in a total rate of 344 Hz for the background and ~ 0.3 Hz for $\Lambda_b^0 \to J/\Psi\Lambda^0$, which is also an upper limit for the rates of the other channels.

Another way to trigger the decays are exclusive lines, where the whole decay is needed for a positive trigger decision. While the signal efficiency stays approximately the same, the background rate is further reduced by a factor of three to seven for the different channels. So the exclusive lines reject more background, but the inclusive line is capable of storing data for many different channels with the same endparticles and also of discovering new channels.

Although the used selections are improvable, the observed efficiencies and a higher multiplicity will lead to higher statistics for Run III, which will get us another step closer to an amplitude analysis with the ultimate goal to search for a pentaquark with strangeness.

Bibliography

[1] G. Aad, T. Abajyan, B. Abbott, *et al.*, "Observation of a new particle in the search for the Standard Model Higgs boson with the ATLAS detector at the LHC," *Physics Letters, Section B: Nuclear, Elementary Particle and High-Energy Physics*, vol. 716, no. 1, pp. 1–29, 2012.

[2] S. Chatrchyan, V. Khachatryan, A. M. Sirunyan, *et al.*, "Combined results of searches for the standard model Higgs boson in pp collisions at s=7 TeV," *Physics Letters, Section B: Nuclear, Elementary Particle and High-Energy Physics*, vol. 710, no. 1, pp. 26–48, 2012.

[3] M. Gell-Mann, "A schematic model of baryons and mesons," *Physics Letters*, vol. 8, no. 3, pp. 214–215, 1964.

[4] R. Aaij, B. Adeva, M. Adinolfi, *et al.*, "Observation of J $/\psi$p Resonances Consistent with Pentaquark States in Λb0 $\to$j $/\psi$K-p Decays," *Physical Review Letters*, vol. 115, no. 7, pp. 1–15, 2015.

[5] C. Vahl, "First observation of the decay $\lambda_b^0 \to j/\psi^0\varphi$ with the lhcb experiment (unpublished)," 2017.

[6] "Internet source: CERN: The standard model." `https://home.cern/about/physics/standard-model`. Last time visited 11.10.2018.

[7] M. Kobayashi and T. Maskawa, *CP-Violation in the Renormalizable Theory of Weak Interaction*. 1973.

[8] S. Behrends, S. Belforte, G. Bellettini, *et al.*, "Observation of Top Quark Production in ‾ pp Collisions," 1995.

[9] "Internet source: Picture of the fundamental particles." `https://en.wikipedia.org/wiki/Standard_Model#/media/File:Standard_Model_of_Elementary_Particles.svg`. Last time visited 11.10.2018.

[10] "Internet source: Picture of the $S = \frac{1}{2} baryon octet$." `https://en.wikipedia.org/wiki/File:Baryon_octet.svg`. Last time visited 11.10.2018.

[11] H. J. Lipkin, "New possibilities for exotic hadrons — anticharmed strange baryons," *Physics Letter B*, vol. 195, no. 3, 1987.

[12] T. Nakano, D. S. Ahn, J. K. Ahn, *et al.*, "Evidence for a Narrow $S = +1$ Baryon Resonance in Photoproduction from the Neutron," *Physical Review Letters*, vol. 91, no. 1, pp. 1–4, 2003.

[13] "Doubt in cast on pentaquarks," *Nature*, 2005.

[14] A. Feijoo, V. K. Magas, A. Ramos, *et al.*, "A hidden-charm S=-1 pentaquark from the decay of Λbinto J/$\psi\eta$Λ states," *European Physical Journal C*, vol. 76, no. 8, pp. 1–12, 2016.

[15] J. X. Lu, E. Wang, J. J. Xie, *et al.*, "Λb →j /ψK0 Λ reaction and a hidden-charm pentaquark state with strangeness," *Physical Review D*, vol. 93, no. 9, 2016.

[16] R. Aaij, B. Adeva, M. Adinolfi, *et al.*, "Amplitude analysis of $B^+ \rightarrow J/\psi\phi K^+$ decays," vol. 012002, no. September, 2016.

[17] "Internet source: Particle Data Group (PDG)." `http://pdg.lbl.gov/`. Last time visited 11.10.2018.

[18] R. Aaij, A. Affolder, K. Akiba, *et al.*, "Performance of the LHCb Vertex Locator," *Journal of Instrumentation*, vol. 9, no. 9, 2014.

[19] "Internet source: LHCb public: Magnet." `https://lhcb-public.web.cern.ch/lhcb-public/en/Detector/Magnet-en.html`. Last time visited 11.10.2018.

[20] M. Adinolfi, G. Aglieri Rinella, E. Albrecht, *et al.*, "Performance of the LHCb RICH detector at the LHC," *European Physical Journal C*, vol. 73, no. 5, pp. 1–17, 2013.

[21] "Internet source: LHCb public: Calorimeter." `https://lhcb-public.web.cern.ch/lhcb-public/en/Detector/Calorimeters-en.html`. Last time visited 11.10.2018.

[22] A. A. A. Jr, L. Anderlini, M. Anelli, *et al.*, "Performance of the LHCb muon system,"

[23] "Internet source: LHCb public: Muons." `https://lhcb-public.web.cern.ch/lhcb-public/en/Detector/Muon2-en.html`. Last time visited 11.10.2018.

[24] "Internet source: Picture of the LHCb detector along the bending plane." `https://en.wikipedia.org/wiki/LHCb_experiment#/media/File:Lhcbview.jpg`. Last time visited 11.10.2018.

[25] R. Aaij, J. Albrecht, F. Alessio, *et al.*, "The LHCb trigger and its performance in 2011," *Journal of Instrumentation*, vol. 8, no. 4, 2013.

[26] "Internet source: The LHCb run 2 data flow." `https://lhcb.github.io/starterkit-lessons/first-analysis-steps/img/lhcb_run_2_data_flow.png`. Last time visited 11.10.2018.

[27] LHCb, "LHCb Trigger and Online TDR," no. May, 2014.

[28] "Studies of $\lambda_b^0 \to J/\psi\lambda$ production in pp collisions at $\sqrt{s} = 7$ tev," Oct 2012. Linked to LHCb-ANA-2011-106.

[29] R. Aaij, B. Adeva, M. Adinolfi, *et al.*, "Study of the production of Λ_b^0 and $\bar{B}^0$ hadrons in pp collisions and first measurement of the $\Lambda_b^0 \to J/\Psi p K^-$ branching fraction ," *Chinese Physics C*, vol. 40, no. 1, p. 011001, 2016.

[30] R. Aaij, B. Adeva, M. Adinolfi, *et al.*, "Measurement of the b -Quark Production Cross Section in 7 and 13 TeV pp Collisions," *Physical Review Letters*, vol. 118, no. 5, pp. 1–11, 2017.

Acknowledgments

Erklärung

Ich versichere, dass ich diese Arbeit selbstständig verfasst und keine anderen als die angegebenen Quellen und Hilfsmittel benutzt habe.

Heidelberg, den